Modelling Simul. Mater. Sci. Eng. 1 (1993) 189–201. Printed in the UK

# Thermodynamic properties of small zinc clusters based on atomistic simulations

R Ramprasad and R G Hoagland†
Department of Mechanical and Materials Engineering, Washington State University, Pullman, WA 99164, USA

Received 23 June 1992, accepted for publication 21 August 1992

**Abstract.** Molecular-dynamics calculations were performed on zinc atom clusters to determine their equilibrium configurations using an embedded-atom method (EAM) potential developed for zinc. Calculation of the thermodynamic properties at different temperatures involved a Monte Carlo scheme in conjunction with statistical mechanical techniques. The harmonic approximation was used in the calculation of the vibrational contribution to the cluster partition function and the rigid-body approximation was used in the calculation of the rotational contribution. The above calculations were used to examine the Helmholtz free energy of formation of the clusters as a function of cluster size, temperature and pressure with the aim of determining the nucleation rates and critical supersaturation pressures. Three cluster-growth patterns were considered in all the above calculations and stability diagrams were plotted indicating the relative stability of clusters as a function of cluster size and temperature for these three growth patterns.

## 1. Introduction

In recent years, considerable interest has been focused on materials with ultrafine microstructures [1] with the anticipation that their properties will be superior to conventional materials that have phase or grain structures on a coarser size scale. Such materials with nanoscale grain sizes are called nanocrystalline materials and can be assembled from clusters of atoms (nanoclusters) typically composed of a few to a few thousand atoms. Recently, considerable research has been done on the synthesis and characterization of gas condensed nanophase metals and ceramics [2–5]. There has also been increasing interest in the nanoclusters themselves at the atomic level.

Part of the motivation for studying clusters is the desire to understand how physical properties evolve in the transition from atom to cluster to small pieces of the bulk solid. Another motivation is associated with questions arising from the desire to use smaller and smaller solid structures in technological applications. Because of the variety of fields in which interest in clusters has arisen, approaches to their study vary considerably. In some fields of chemical physics, one example being nucleation theory, the thermodynamic properties of small clusters are of great importance. The development of fast computers has allowed investigators to model these properties by atomic simulations. Total-energy calculations can be used to predict the structural arrangements and properties of clusters.

† e-mail: hoagland @ honcho.mme.wsu.edu

0965-0393/93/020189+13$07.50  

There are essentially two types of approaches to these calculations, *ab initio* and empirical. The former provides more or less exact solutions via some version of Hartree–Fock formalism. The latter employs interatomic interaction potentials that are empirical in nature. In the case of *ab initio* calculations, one is less concerned with limitations imposed on the accuracy than on the size of the cluster, and *vice versa* for calculations based on empirical potentials. *Ab initio* calculations require quite significant resources when the system involves more than about 200 electrons, although this number is increasing as faster (e.g. massively parallel) computers become available. On the other hand, the advantage of empirical potentials is that such resource limitations are not encountered until the system sizes exceed about $10^4$–$10^5$ atoms. Our interest here concerns zinc clusters with too many atoms to be amenable to treatment by *ab initio* calculations, and therefore, we have employed a type of potential based on the embedded-atom method (EAM) [6–8].

Some early studies made use of pairwise potentials to determine the relative energies of small clusters of identical atoms. Using static relaxation, Hoare and Pal [9] identified several growth sequences for the formation of small clusters of argon atoms. A formal physical-cluster theory of cluster nucleation has been put forward by Lee, Barker and Abraham [10]. Molecular-dynamics calculations have also been performed on Lennard-Jones argon clusters by McGinty [11] over a wide range of sizes and temperatures. More recently, the thermodynamics and nucleation of small clusters of aluminum atoms were studied using an interatomic potential obtained by the EAM by Ramprasad and Hoagland [12].

Pair potentials, while yielding the total energy directly, require the use of an accompanying volume-dependent energy term to properly describe the elastic properties of metals. The presence of free surfaces creates special difficulties in applying such a volume-dependent energy. In addition, in the case of metallic systems, the interaction between atoms is intrinsically many-body in nature. The above considerations have lead to the evolution of many-body potentials.

In the present work, an EAM interatomic potential for zinc was developed. The procedure involved is described in the first section of this paper. Molecular-dynamics techniques were then used to study zinc clusters to find their equilibrium configurations (most stable configurations at absolute zero) and also to study the structural geometry of the very small clusters. A Monte Carlo scheme was used to find their configuration at temperatures other than absolute zero, statistical mechanical techniques were used to evaluate the Helmholtz free energy of formation of the clusters and eventually the nucleation rates were calculated at different temperatures. Partition functions are separated and all degrees of freedom are explicitly considered. As a result the translation–rotation paradox [13], which arises due to neglecting the translational and rotational terms, is taken care of. Further, as solid clusters are dealt with here, ambiguities associated with the liquid drop vanish. Though the extremely high surface-to-volume ratio of the very small clusters is prone to create difficulties, the EAM potential used here (which is typically designed to study bulk material properties) is shown to suggest some interesting properties of zinc clusters.

## 2. The potential

Daw and Baskes developed the embedded-atom method, a technique based on local electron-density theory, for the construction of many-body potentials for metals. The

method describes the potential energy of an atom in a crystal as the sum of a long-range embedding energy, and a short-range pair potential. The embedding energy arises from the change of the energy of an electron gas when ion cores are embedded in the electron gas. The EAM functional form for calculating the energy of an atom is given by [14, 15]

$$E_i = F_i(\rho_i) + \tfrac{1}{2}\sum_{j\neq 1}\phi_{ij}(r_{ij}) \tag{1}$$

where

$$\rho_i = \sum_{j\neq 1} f_j(r_{ij}) \tag{2}$$

$E_i$ is the potential energy associated with atom $i$, $\rho_i$ is the total electron density at atom $i$ due to the rest of the atoms in the system, $F_i(\rho_i)$ is the energy required to embed atom $i$ into the electron density $\rho_i$, $\phi_{ij}(r_{ij})$ is the pair potential between atoms $i$ and $j$ separated by the distance $r_{ij}$, and $f_i(r_{ij})$ is the contribution to the electron density of $i$ due to the presence of $j$. In the case of zinc, the summation included contributions up to the fifth-nearest neighbours. In order to apply the EAM, the $f$, $\phi$ and $F$ functions must be known. The standard fitting procedure to determine these functions is to choose specific functional forms for $f$ and $\phi$, to determine the parameters of $f$ and $\phi$ by fitting to experimental data and finally to determine $F$ by Foiles' [16] scheme.

An exponential functional form is chosen for $f$

$$f(r) = \exp\left[-\beta(r/r_e - 1)\right] \tag{3}$$

where $r_e$ is the equilibrium interatomic separation. From the free-atom electron-density data tabulated in the Clementi and Roetti double zeta tables [17], the spherically averaged electron-density distribution around an atom is determined as a function of the distance from the centre of the atom. The total electron density was taken to be a linear sum of the s electron contributions. Figure 1 shows the electron density and a least-squares fit of equation (3) that yields $\beta = 7.34$ for $r_e = 2.665$ angstroms.

In order to get the pair potential, the bulk and shear moduli, the lattice parameter,

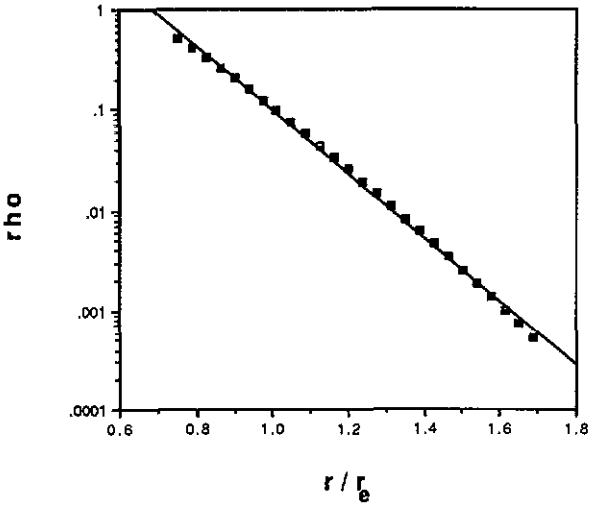


**Figure 1.** The spherically averaged free-atom electron density data obtained from Clementi and Roetti tables for zinc; the least squares fit represented by the straight line for which $\rho = \exp\left[-\beta(r/r_{e-1})\right]$ gave $\beta = 7.34$.

the $c/a$ ratio and the energy of formation of a single vacancy are used for fitting. The equations relating the equilibrium properties such as the cohesive energy ($E_c$) and the linear elastic constants ($C_{ijkl}$) to the EAM parameters are dealt with extensively in the literature [11, 14]. For HCP metals with $c/a$ ratio less than or equal to the ideal value, the usual method to obtain the pair potential is to assume an exponential form similar to that of the electron density. However, difficulties were encountered (i.e. the lattice equilibrium condition could not be solved when an exponential functional form was chosen for $\phi$) when a similar procedure was adopted for zinc which has a $c/a$ ratio much greater than ideal. As a result, a slightly different procedure which introduces a function called the effective pair potential, was adopted. A fourth-order polynomial was selected to represent his effective pair potential instead of an exponential form. This form with its five coefficients to be determined from various physical properties avoids the computational difficulties of the exponential form.

Starting from equation (1), the argument develops as follows. The equilibrium electron density is added and subtracted from the total electron density and the total energy is written as a Taylor series expansion about the equilibrium electron density

$$\begin{aligned} E_{\text{tot}} &= \sum_i F_i\left(\sum_j f(r_{ij})\right) + \tfrac{1}{2}\sum_{ij,i\neq j}\phi_{ij}(r_{ij}) \\ &= \sum_i F_i\left(\rho_e + \left(\sum_j f(r_{ij}) - \rho_e\right)\right) + \tfrac{1}{2}\sum_{ij,i\neq j}\phi_{ij}(r_{ij}) \\ &\approx \sum_i [F_i(\rho_e) - \rho_e F_i'(\rho_e)] + \tfrac{1}{2}\sum_{ij,i\neq j} 2F_i'(\rho_e) f(r_{ij}) + \tfrac{1}{2}\sum_{ij,i\neq j}\phi_{ij}(r_{ij}) \\ &\approx \sum_i [F_i(\rho_e) - \rho_e F_i'(\rho_e)] + \tfrac{1}{2}\sum_{ij,i\neq j}\psi_{ij}(r_{ij}) \end{aligned} \tag{4}$$

where

$$\psi(r_{ij}) = 2F_i'(\rho_e) f(r_{ij}) + \phi_{ij}(r_{ij})$$

is an effective pair potential. Also, the EAM potential is invariant to a transformation in which a term linear in the electron density is added to or subtracted from the embedding function. Making an appropriate adjustment to the two-body potential, i.e., the transformation

$$\begin{aligned} F(\rho_e) &\Leftrightarrow F(\rho_e) + t\rho_e \\ \phi(r_e^m) &\Leftrightarrow \phi(r_e^m) - 2tf(r_e^m) \end{aligned}$$

makes no change in the potential. One can always choose the constant $t$ so that $F'(\rho_e)$ is zero and as a result $\psi(r) = \phi(r)$. It can be shown that certain properties that are used for fitting can be expressed, after some algebraic manipulations, solely in terms of the effective pair potential in a very general manner. Also, if we decide to choose $F'(\rho_e) = 0$, then we can merely replace $\psi(r)$ by $\phi(r)$. According to the above treatment, and following the derivations in [14], the lattice parameter, the $c/a$ ratio, the bulk and shear moduli and the single-vacancy formation energy are related to the pair potential as follows:

(i) the lattice parameter and $c/a$ ratio are related to the pair potential in

$$\sum_m \left( \frac{x_e^m x_e^m}{r_e^m} + \frac{z_e^m z_e^m}{r_e^m} \right) \phi'(r_e^m) = 0 \tag{6}$$

(ii) the bulk modulus $B$ is given by

$$[F''(\rho_e)\,(r_e^m \rho_e')^2 + \tfrac{1}{2}\sum_m (r_e^m)^2 \phi''(r_e^m)] = 9\,\Omega_e\,B \tag{7}$$

(iii) the shear modulus $G$ is given by

$$[F''(\rho_e)\,(r_e^m \rho_e')^2 (1 - 3Q) + \tfrac{1}{2}\sum_m (r_e^m)^2 \phi''(r_e^m)] = 15\,\Omega_e\,G \tag{8}$$

(iv) the single-vacancy formation energy is approximately given by

$$\tfrac{1}{2}\phi(r_e^m) \approx -E_{1v}^{uf}. \tag{9}$$

In the above

$$\rho_e' = \sum_m \left( \frac{r_e^m}{r_e} \right) f'(r_e^m)$$

$$Q = q_1 q_2 + q_2 q_3 + q_3 q_1$$

$$q_i = \left\{ \sum_m [(r_{i,e}^m)^2 / r_e^m]\, f'(r_e^m) \right\} / (r_e \rho_e').$$

The sums are over the $m$ neighbours and $\Omega_e$ is the equilibrium atomic volume.

Equations (7) and (8) can be combined to eliminate $F''(\rho_e)$

$$\frac{3Q}{2}\sum_m (r_e^m)^2 \phi''(r_e^m) = 15\,\Omega_e\,G - 9(1 - 3Q)\Omega_e\,B. \tag{10}$$

In addition, we have imposed the condition that both potentials go smoothly to zero at the cut-off distance, so that

$$\phi(r_{cut}) = 0 \tag{11}$$

$$\phi'(r_{cut}) = 0. \tag{12}$$

We choose the following functional form for $\phi$

$$\phi(r) = K_4(r/r_e - 1)^4 + K_3(r/r_e - 1)^3 + K_2(r/r_e - 1)^2 + K_1(r/r_e - 1) + K_0 \tag{13}$$

and solve for the five coefficients using equations (6), (19)–(12). Figure 2 shows a plot of the pair potential versus the scaled interatomic distance for a cut-off distance of 4.84 Å (between the fifth- and sixth-nearest neighbours). The plot indicates that the pair potential is highly repulsive for interatomic distances that are much smaller than the equilibrium nearest-neighbour distance, attractive for distances in the vicinity of the equilibrium nearest-neighbour distance and repulsive for larger distances and goes to zero smoothly at the cut-off. It was observed that the pair potential varied drastically with the cut-off; some values of the cut-off, in fact, yielded unrealistic relationships between the pair potential and interatomic distance where the pair potential was highly attractive for very small interatomic separations and repulsive for large separations.

Finally, the embedding energy is determined as a function of $r$ using Foiles' scheme,

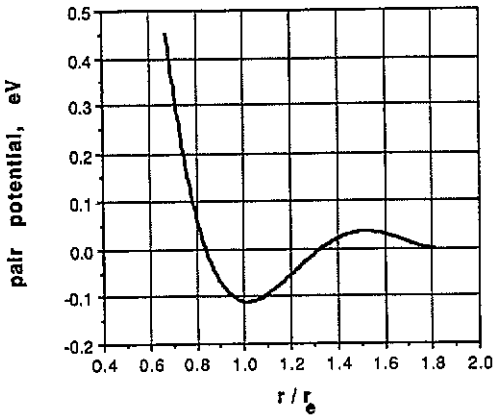


**Figure 2.** The effective pair potential versus the scaled interatomic distance with the cut-off at 4.84 Å.

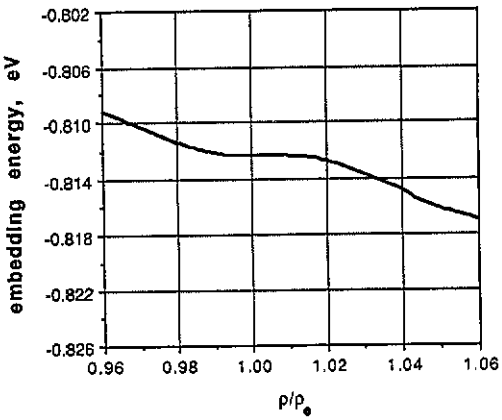


**Figure 3.** Plot of the embedding energy as a function of the scaled electron density for zinc.

by uniformly dilating the lattice and calculating the resultant energy change from a universal equation of state given by Rose *et al* [18]

$$E(a) = -E_c[1 + \alpha(a/a_0 - 1)] \exp(-\alpha(a/a_0 - 1)) \tag{14}$$

where $\alpha$, the reduced lattice parameter is given by $\alpha = 3(\Omega_e B/E_c)$ and $a$ is the lattice parameter. Using equations (1) and (14) $F(\rho)$ is obtained. The pair potential is obtained for several values of the cut-off distance; using the calculated pair potential and the total energy given by equation (14), the embedding energy is evaluated. The elastic constants are then calculated with this potential; the cut-off which results in a minimum deviation of the calculated elastic constants from the experimental values is determined; the potential which is based on this particular cut-off is the one that is used in subsequent calculations. Figure 3 shows the dependence of the embedding energy on the scaled electron density for zinc. Figure 4 shows the total potential energy per atom for zinc ($c/a = 1.85629$) as a function of the lattice parameter $a$.

Zinc, a HCP metal, has five independent single crystal elastic constants. These elastic constants were calculated [11, 14] using the EAM potential developed for zinc. Figure 5

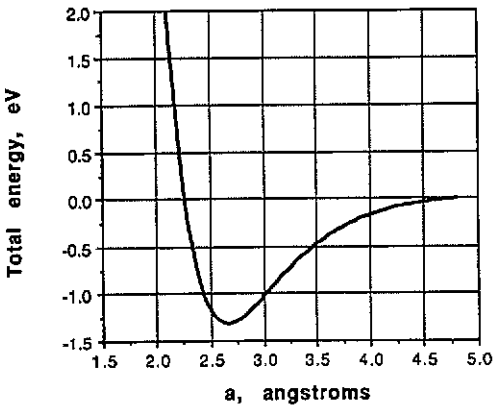


**Figure 4.** Variation of the total energy per atom with the lattice parameter, $a$, for zinc ($c/a = 1.85629$) as given by the Rose equation of state.

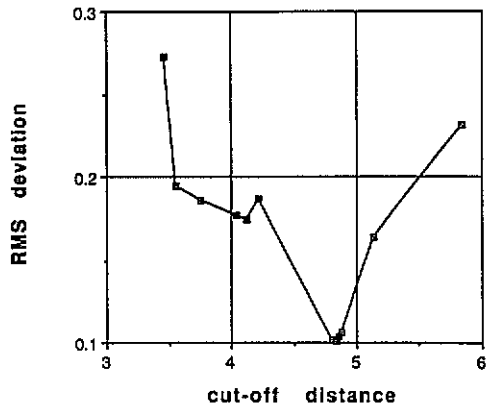


**Figure 5.** Dependence of the root mean square deviation of the predicted elastic constants from the experimental values on the cut-off distance for zinc.

**Table 1.** Physical properties of zinc. All energies are in eV, distances in Å and elastic constants, bulk and shear moduli in $eV Å^{-1}$.

| Inputs used for fitting in equations (6), (9)–(12) and (14) | | |
|---|---|---|
| $a$ | 2.665 | |
| $c/a$ | 1.85629 | |
| $E_{lv}^{uf}$ | 0.5 | |
| $\langle B \rangle_v$ | 0.4381 | |
| $E_c$ | 1.35 | |
| Elastic constants | Experimental | Calculated |
| $C_{11}$ | 0.9891 | 0.9565 |
| $C_{12}$ | 0.1969 | 0.3432 |
| $C_{13}$ | 0.2965 | 0.2190 |
| $C_{33}$ | 0.385 | 0.4677 |
| $C_{44}$ | 0.25 | 0.3735 |
| $\langle G \rangle_v$ | 0.2845 | 0.3174 |

shows the variation of the root-mean-square deviation of the predicted elastic constants from the experimental ones with the cut-off. Certain elastic constants, $C_{33}$ in particular, varied quite drastically with the cut-off. From figure 5 it can be noted that the RMS deviation was minimum for a cut-off distance of 4.84 Å on which the potential for Zn that was used in subsequent calculations was based. Table 1 compares experimental values of various properties with those predicted by the EAM potential. It can be seen that, with the exception of $C_{12}$, there is reasonable agreement in the elastic constants.

## 3. Computational procedure

Clusters which were part of the HCP, FCC and icosahedral lattices were generated and relaxed to equilibrium at 0 K by a molecular-dynamics technique [19]. It is worth mentioning here that an icosahedron (figure 6) is a geometric structure that has 12 vertices and 20 faces and has six 5-fold symmetry axes. To get the cluster configurations at temperatures other than 0 K, a Metropolis Monte Carlo scheme [20] was used to obtain the expectation values of the coordinates of the cluster atoms, the average potential energies and the principal moments of inertia at a temperature $T$. The procedure begins with an equilibrium ($T \sim 0$ K) cluster and from this a Boltzmann-weighted set of configurations is generated by random displacements of the atoms in the cluster. The following results were based on 10 000 such configurations which were accumulated for averaging for each temperature of the simulation.

The partition function of a cluster is evaluated in the same way one would evaluate

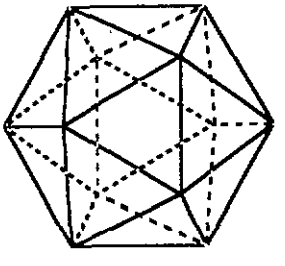

**Figure 6.** An icosahedron.

that of a polyatomic molecule. The cluster Hamiltonian is assumed to be separable:

$$H = H_{\text{vib}} + H_{\text{rot}} + H_{\text{tr}} \tag{15}$$

enabling the cluster partition function to be written as a product

$$q = q_{\text{vib}} q_{\text{rot}} q_{\text{tr}}. \tag{16}$$

The individual terms in the product are evaluated from standard statistical mechanical formulas using the harmonic approximation to evaluate the vibrational component $q_{\text{vib}}$, the rigid-rotor approximation to evaluate the rotational component $q_{\text{rot}}$, and the perfect-gas approximation to evaluate the translational component $q_{\text{tr}}$.

$$q_{i,\text{vib}} = \exp\left(\frac{U}{kT}\right) \prod_{j=1}^{3i-6} \frac{\exp\left(-h\vartheta_j/2kT\right)}{1 - \exp\left(-h\vartheta_j/kT\right)} \tag{17}$$

$$q_{i,\text{rot}} = \left(\frac{\pi^{1/2}}{\sigma}\right)\left(\frac{8\pi^2 kT}{h^2}\right)^{3/2} (I_{\text{A}} I_{\text{B}} I_{\text{C}})^{1/2} \tag{18}$$

$$q_{i,\text{tr}} = \left(\frac{n_i kT}{P_i}\right)\left(\frac{2\pi mikT}{h^2}\right)^{3/2} \tag{19}$$

where $P$ is the partial pressure of $i$-atom clusters, $m$ is the mass of a single atom, $h$ is Planck's constant, $U$ the averaged potential energy of the cluster and $I_{\text{A}}$, $I_{\text{B}}$, $I_{\text{C}}$, the principal moments of inertia. The vibrational partition function is calculated by normal mode analysis. This involves diagonalization of the force-constant matrix whose elements are for an $i$-atom cluster, the $(3i)^2$ second derivatives of the cluster's equilibrium potential energy [21]. The elements of the force-constant matrix are evaluated by inserting equilibrium coordinate values of the atoms into the above analytic expression for the second derivatives. The normal frequencies of oscillation are obtained from the eigenvalues $\omega_j^2$ of this matrix by the relation $2\pi\nu_j = \omega_j$. These partition functions are used to calculate the Helmholtz free energy of formation of the cluster as

$$A(i, T) = -kT \ln (q). \tag{20}$$

Since our motivation in this work stems primarily from interest in determining the critical conditions for nucleation of clusters from the vapour, the quantity that is eventually calculated is the critical supersaturation pressure, the pressure at which the vapour becomes metastable relative to an $i$-atom cluster. To calculate the critical value, and equilibrium theory of rates is assumed. The critical supersaturation pressure is identified as the pressure at which the rate of nucleation becomes large. In practice, this identification of the critical supersaturation pressure can be made with little ambiguity since the calculated rate increases quite drastically from a very small to a very large value as the pressure is increased through the critical value. The steady-state rate of nucleation was calculated as

$$J = [P/(2\pi mkT)^{1/2}] S(i^*) c_1 (\Delta A^*/3\pi kTi^{*2})^{1/2} \exp\left(-\Delta A^*/kT\right) \tag{21}$$

where $i^*$ is the size, $S(i^*)$ the surface area and $\Delta A^*$ the Helmholtz free energy of formation of the cluster with the largest free energy of formation.

## 4. Results and discussion

### *4.1. Clusters at 0 K*

As mentioned before, each equilibrium cluster is formed by relaxing a non-equilibrium cluster. The most stable 4-atom cluster is found to be the one having a dense regular tetrahedral structure as shown in figure 7. We note that certain other approaches such as the self-consistent local spin density (LSD) calculations [22], or the generalized valence bond (GVB) approach [23] give different results in that they predict the 4-atom Na and Li clusters with a planar-rhombus geometry to be more stable. This geometry is not likely to emerge as a stable one for an EAM model because there an intrinsic dependence on bond angle is needed to favour a rhombus over a tetrahedron but this is a feature lacking in the EAM potential. The most stable 5-atom cluster was the one obtained when an atom was placed on one of the faces of the tetrahedral 4-atom cluster.

From this point on, to generate clusters in a systematic way, and since clusters with more than five atoms have at least one metastable configuration, three distinct symmetry patterns, namely HCP, FCC and icosahedral were followed.

An octahedral cluster is the most stable 6-atom cluster. This is an FCC close-packed structure as shown in figure 7. The first instance of a cluster with the geometric structure of a pentagonal bipyramid is a 7-atom cluster which falls in the category of icosahedral clusters, since a pentagonal bipyramid is part of an icosahedron. A picture of a 7-atom cluster is shown in figure 7. Five regular tetrahedra fit almost perfectly around a common edge to form a pentagonal bipyramid, but not quite; some distortion (about a 1% change in bond angle and bond length) is necessary in each of the tetrahedra in

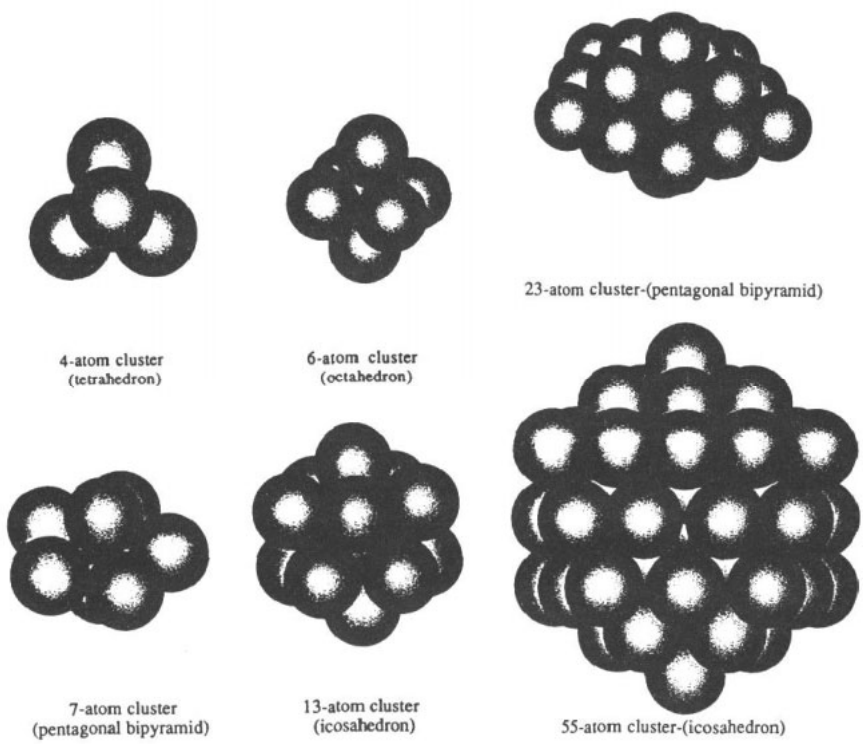


**Figure 7.** Equilibrium clusters.

order to make a perfect fit. This is also the reason why the basic building block of an icosahedral packing is a distorted tetrahedron. This 7-atom pentagonal bipyramidal cluster was quite stable and, in fact, the 7-atom FCC cluster was unstable relative to the icosahedral geometry. As a further indication of the relative stability of the icosahedral lineage, there is a very large drop in energy per atom on going from 6- to 7-atoms as shown in figure 8. The most stable 8-atom cluster also had icosahedral symmetry with a substantially smaller drop in energy per atom than the 6- to 7-atom step indicating that the 7-atom cluster is a particularly stable structure. It is also interesting to note that the energy per atom of HCP 6- and 7-atom clusters was higher than that of the 5-atom cluster. Mention of this will be made later when discussing free energy and nucleation-kinetics considerations. The most stable clusters with atoms from 9 to 14 had icosahedral symmetry; the energy difference between the 12- and 13-atom clusters was much greater than that between the 13- and 14-atom clusters; the reason for this is that the 13-atom cluster is the smallest cluster with an atom not on the surface. The 13-atom icosahedral cluster, shown in figure 7, has a potential energy which is about 3.5% less than that of the corresponding HCP cluster. The most stable 15-atom cluster was a HCP cluster. From this point on, the icosahedral configuration was most preferred for clusters up to 57 atoms.

It is worthwhile to examine some clusters which have closed-shell configurations and other types of special symmetry. HCP clusters with 19-, 21-, 39-, 51- and 57-atoms have completely filled second, third, fourth, fifth and sixth shells respectively; of the FCC clusters, the 19-, 43- and 55-atom clusters have fully filled second, third and fourth shells. The above may suggest that these clusters could have the lowest energy, but calculations show that the icosahedral clusters (as large as 57 atoms/cluster) are the ones which have lowest energy for clusters with more than 6 atoms at 0 K.

The 23-atom icosahedral cluster (the most stable 23-atom cluster) has the geometry of a pentagonal bipyramid as shown in figure 7. Another cluster of interest is the lowest energy 55-atom cluster, also shown in figure 7, which has the geometric structure of an icosahedron; this cluster has a filled third shell in this geometry while the 13-atom icosahedral cluster has a filled first shell. Figure 8 shows the potential energy per atom of zinc clusters versus the number of atoms per cluster from which it is evident that

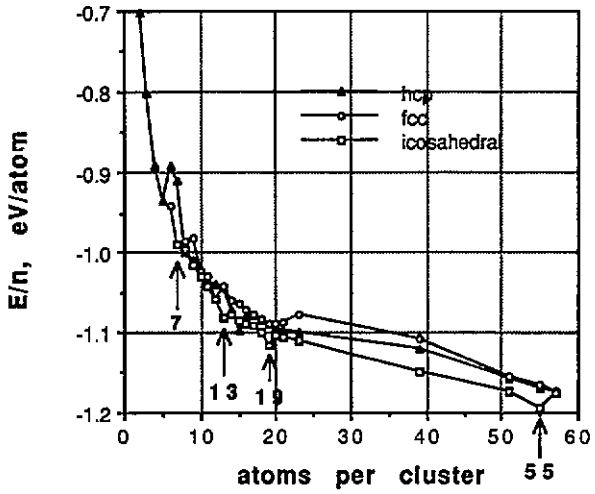


**Figure 8.** Potential energy per atom of Zn clusters versus numbers of atoms per cluster for three types of symmetry patterns.

clusters with 7, 13, 19, 55 atoms exhibit special stability. These numbers — 7, 13, 19, 55 — are referred to as magic numbers.

### *4.2. Nucleation of clusters from vapour*

The free energies of formation of the clusters were calculated from

$$\Delta A(i, T, P) = \Delta A^0(i, T) + (1 - i)kT \ln P \tag{22}$$

where

$$\Delta A^0(i, T) = A^0(i, T) - nA^0(1, T) \tag{23}$$

is the standard Helmholtz free energy of formation of an $i$-atom cluster. $A^0(1, T)$ is the free energy of a 1-atom cluster which is the gas and is given by

$$A^0(1, T) = -kT \ln (q_{1,\mathrm{tr}}). \tag{24}$$

The standard free energy of formation of zinc clusters at 1650 K for HCP, icosahedral and FCC growth schemes as a function of cluster size is given in figure 9. It can be seen that the free energy of formation of the 7-atom HCP cluster is more than twice as large as that of the 7-atom icosahedral cluster. The fact that the 7-atom HCP cluster is so unstable when compared to the 7-atom icosahedral cluster is, to a large extent, suggestive of a high nucleation barrier to the growth of the HCP clusters. This will be discussed below. The low stability of this particular HCP cluster only supports the earlier results, obtained at 0 K by molecular dynamics calculations, that the 7-atom HCP cluster has higher potential energy per atom than the 5-atom cluster.

The free energy of formation was studied as a function of the number of atoms per cluster in the temperature range 1450 K–1650 K. The trend that was noticed was that the most stable 6-atom cluster was a FCC cluster; for clusters with more than 6 atoms but 13 or less atoms the icosahedral clusters were the most stable. Thereafter, the HCP clusters were the ones with lowest free energy of formation with the exception of the 16-atom cluster, in which case the icosahedral symmetry was preferred. Nucleation rates were then calculated as a function of temperature and pressure and subsequently the critical supersaturation pressures were identified at different temperatures as those pressures at which the nucleation rates increased from a very small to a very large value. Figure 10 shows the dependence of the critical supersaturation pressure on temperature for the HCP, FCC and icosahedral zinc clusters. As was expected the nucleation kinetics favoured the HCP and FCC growth patterns least.

The free energy curves were then used to plot stability diagrams at 1 atm. and 0.5 atm. as shown in figure 11. It is evident that though small icosahedral clusters are more strongly favoured at low temperatures, the HCP configuration having more than 13 atoms (with the exception of the 16-atom cluster) is more stable at higher temperatures. At temperatures close to absolute zero, the icosahedral configuration could be stable for zinc clusters having up to at least 57 atoms; however, as the temperature is increased, the HCP structure is entropically favoured and so the HCP clusters become stable. The EAM version of zinc as presented here has a slightly higher boiling point than the actual value. The boiling point of Zn is about 1400 K as predicted by these calculations when compared to the actual boiling point which is 1180 K. It is also worth noting that the features present in this diagram are not simply characteristic of the EAM, since, in a similar study by us [12] on EAM aluminum clusters, the corresponding phase diagram was considerably different, showing much less structure than here.

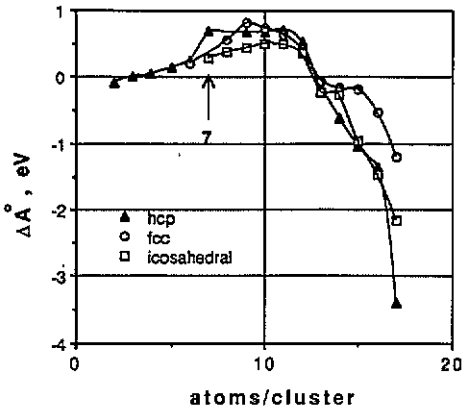


**Figure 9.** Standard free energy of formation of zinc clusters as a function of the number of atoms per cluster at $T = 1650K$.

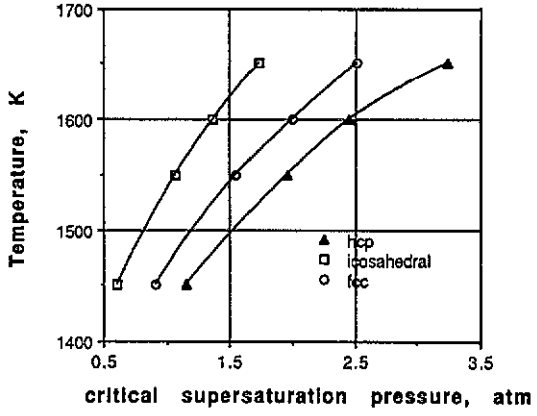


**Figure 10.** Temperature versus the critical supersaturation pressure for zinc clusters.

In the above discussion, several model calculations of clusters using an EAM potential were presented. As was just mentioned, such calculations inevitably contain elements of uncertainty associated with the potentials, approximations due to ignoring the effects of vibrational anharmonicity and the steady-state approximations involved in the calculation of the nucleation rates. However, calculations of the type reported here are instructive and are the first step in the development of understanding of clusters on an atomic level. An approach on this level helps to reduce uncertainties and ambiguities concerning the exact nature of micro clusters.

## 5. Summary

Results that were obtained in the present study can be summarized as follows.

(i) Icosahedral short-range order is strongly favoured at temperatures close to absolute zero in the small clusters of zinc atoms having up to 57 atoms; clusters with 7, 13, 19, 55 (magic numbers) atoms exhibited special stability.

(ii) The study of critical supersaturation pressure as a function of temperature indicated that the HCP clusters had the smallest driving force for nucleation. The reason

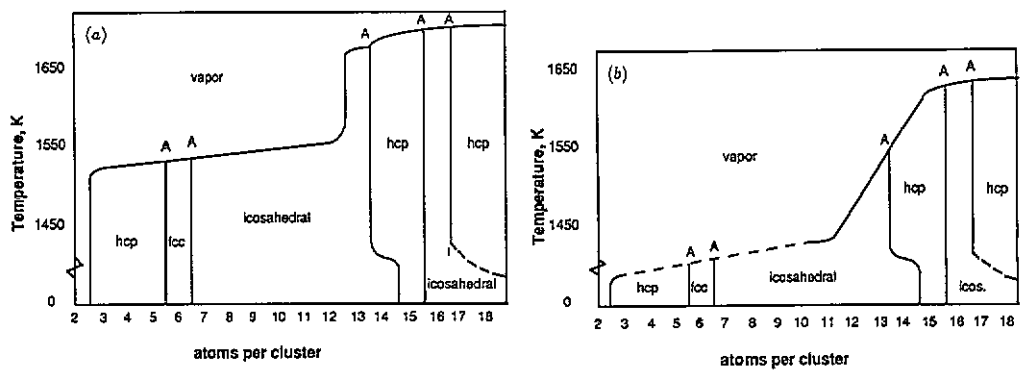


**Figure 11.** Stability diagrams for Zn at (*a*) $P = 1$ atm and (*b*) $P = 0.5$ atm.

for this behaviour was probably due to the low stability of the 7-atom HCP cluster which manifested itself both in the molecular dynamics and the Monte Carlo simulations.

(iii) The stability diagrams showed that, at high temperatures, clusters with more than 13 atoms preferred the HCP configuration; the reason being that the HCP configuration is entropically more favoured at high temperatures.

## Acknowledgments

The authors would like to thank Professor J P Hirth for useful discussions and Dr S M Foiles for his invaluable suggestions. We would also like to express our appreciation for the use of the computing facilities at the Washington State University and for the support of this work by NSF under grant CTS-8912430.

## References

[1] Kear B H, Cross L E, Keem J E, Siegel R W, Spaepen F, Taylor K C, Thomas E L and Tu K N 1989 *Research Opportunities for Materials with Ultrafine Microstructures* vol NMAB-454 (Washington, DC: Natl. Acad. Sci.)
[2] Andres R P, Averback R S, Brown W L, Brus L E, Goddard W A, Kaldor A, Louie S G, Moskovits M, Peercy P S, Riley S J, Siegel R W, Spaepen F and Wang Y 1989 *J. Mater. Res.* **4** 704
[3] Gleiter H 1981 *Deformation of Polycrystals: Mechanisms and Microstructures* ed N Hansen *et al* (Roskilde, Denmark: Risø National Laboratory) p 15
[4] Birringer R, Herr U and Gleiter H 1986 *Trans. Japan. Inst. Met. Suppl.* **27** 43
[5] Siegel R W and Hahn H 1987 *Current Trends in the Physics of Materials* ed M Yussouff p 403
[6] Daw M S and Baskes M I 1984 *Phys. Rev.* **29** 6443
[7] Daw M S and Baskes M I 1983 *Phys. Rev. Lett.* **50** 1285
[8] Baskes M I *et al* February 1988 MRS Bulletin p 28
[9] Hoare M R and Pal P 1971 *Adv. Phys.* **20** 161
[10] Lee J K, Barker J A and Abraham F F 1973 *J. Chem. Phys.* **58** 3166
[11] McGinty D J 1971 *J. Chem. Phys.* **55** 2 580
[12] Ramprasad R and Hoagland R G 1992 Nanocrystalline and nanophase materials *Thermodynamic Properties of Small Clusters of Aluminum Atoms; TMS Conf. Proc. (San Diego, 1992)* at press
[13] Reiss H, Katz J L and Cohen R E 1968 *J. Chem. Phys.* **48** 5553
Lothe J and Pound G M 1968 *J. Chem. Phys.* **48** 1849
[14] Oh D J and Johnson R A 1988 *J. Mater. Res.* **3** 471
[15] Oh D J and Johnson R A 1989 *J. Mater. Res.* **4** 1195
[16] Foiles S M 1985 *Phys. Rev.* B **32** 7685
[17] Clementti E and Roetti C 1974 *Atomic Data Nucl. Data Tables* **14** 177
[18] Rose J H, Smith J R, Guinea F and Ferrante J 1984 *Phys. Rev.* B **29** 2963
[19] Allen M A and Tildesley D J *Computer Simulation of Liquids* (Oxford: Oxford Science Publications)
[20] Metropolis N and Ulam S 1949 *J. Am. Stat. Assoc.* **44** 335
[21] Herzberg G 1950 *Molecular Spectra and Molecular Structure* (New York: Van Nostrand) vol 2
[22] Martins J L, Buttet J and Car R 1985 *Phys. Rev.* B **31** 1804
[23] McAddon M H and Goddard W A 1985 *J. Non-Cryst. Solids* **75** 149; 1987 *J. Phys. Chem.* **91** 2607; 1985 *Phys. Rev. Lett.* **55** 2563